

Equivalence between fermion-to-qubit mappings in two spatial dimensions

Yu-An Chen (陳昱安)^{1,2,*} and Yijia Xu (许逸葭)^{1,3,†}

¹*Department of Physics, Joint Quantum Institute,
and Joint Center for Quantum Information and Computer Science,
NIST/University of Maryland, College Park, Maryland 20742, USA*

²*Condensed Matter Theory Center, University of Maryland, College Park, Maryland 20742, USA*

³*Institute for Physical Science and Technology, University of Maryland, College Park, Maryland 20742, USA*

(Dated: January 14, 2022)

We argue that all locality-preserving mappings between fermionic observables and Pauli matrices on a two-dimensional lattice can be generated from the exact bosonization in Ref. [1], whose gauge constraints project onto the subspace of the toric code with emergent fermions. Starting from the exact bosonization and applying Clifford finite-depth generalized local unitary (gLU) transformation, we can achieve all possible fermion-to-qubit mappings (up to the re-pairing of Majorana fermions). In particular, we discover a new super-compact encoding using 1.25 qubits per fermion on the square lattice, which is lower than any method in the literature. We prove the existence of fermion-to-qubit mappings with qubit-fermion ratios $r = 1 + \frac{1}{2k}$ for positive integers k , where the proof utilizes the trivialness of quantum cellular automata (QCA) in two spatial dimensions. When the ratio approaches 1, the fermion-to-qubit mapping reduces to the 1d Jordan-Wigner transformation along a certain path in the two-dimensional lattice. Finally, we explicitly demonstrate that the Bravyi-Kitaev superfast simulation, the Verstraete-Cirac auxiliary method, Kitaev's exactly solved model, the Majorana loop stabilizer codes, and the compact fermion-to-qubit mapping can all be obtained from the exact bosonization.

CONTENTS

I. Introduction	1
Summary of results	2
II. Super-compact fermion-to-qubit mapping	2
III. Generalized local unitary circuits on the exact bosonization	3
A. Review of the exact bosonization	4
B. Compact fermion-to-qubit mapping with ratio $r = 1.5$	5
C. Super-compact fermion-to-qubit mapping with ratio $r = 1.25$	6
D. General Construction for compact fermion-to-qubit mappings	9
IV. Equivalence between fermion-to-qubit mappings and the exact bosonization	10
A. Bravyi-Kitaev superfast simulation	11
B. Verstraete-Cirac auxiliary method	11
C. Kitaev's honeycomb model	12
D. Majorana loop stabilizer codes	14
E. Connection to Jordan-Wigner transformation	15
Acknowledgement	16
A. Clifford gates	16
References	18

I. INTRODUCTION

A fermion-to-qubit mapping is a duality between local even¹ fermionic operators and local products of Pauli matrices. It is well known that any fermionic system in a 1d lattice can be mapped onto a 1d spin system by the Jordan-Wigner transformation. The Jordan-Wigner transformation can also be applied to systems in higher dimensions by choosing a particular ordering of fermions; however, the mapping becomes highly non-local. From both theoretical and practical points of view, mapping local fermionic operators to local spin operators in higher dimensions is an essential topic. In the last two decades, there have been many proposals of fermion-to-qubit mappings for two dimensions [1–9] and three or arbitrary dimensions [10–12]. These fermion-to-qubit mappings play important roles in various topics of modern physics, such as exactly solvable models for topological phases [3, 13–15], fermionic quantum simulations [2, 4, 5, 8, 10], and quantum error correction [16–21]. In particular, the exact bosonizations in Refs. [1, 7, 11, 12] construct the toric code with fermions in arbitrary dimensions and impose gauge constraints to restrict in the subspace with emergent fermions, which provide an elegant spacetime description by the Chern-Simons and the Steenrod square topological action. The spacetime pictures for other fermion-to-qubit mappings mentioned above are not manifest. Ref. [4] points out that the Verstraete-Cirac auxiliary method [2] can be related to a topological model (toric code), and the compact en-

* E-mail: yuanchen@umd.edu

† E-mail: yijia@umd.edu

¹ We only consider terms respecting the fermion-parity symmetry, i.e., products with even numbers of fermionic creation and annihilation operators.

coding [8] found that its stabilizer is similar to a toric code.

From the theoretical perspective, it is tempting to ask a question: are all fermion-to-qubit mappings in two spatial dimensions “equivalent” to the exact bosonization? First, we define the “equivalence” by finite-depth generalized local unitary (gLU) transformations. Informally speaking, finite-depth gLU transformation is a finite-depth quantum circuit (FDQC) with ancilla qubits. We argue that the answer to the above question is “yes” and demonstrate it with examples.

From the practical point of view, fermion-to-qubit mappings are widely used in fermionic quantum simulations of physical systems. In practical quantum simulations, an important quantity is the qubit-fermion ratio r , the number of qubits to simulate one fermion on average, since it is directly related to the total number of fermionic modes encoded in a qubit array. Suppose we encode n fermionic modes by m qubits, then the qubit-fermion ratio is $\frac{m}{n}$. The best fermion-to-qubit mapping on the 2d square lattice is the compact fermion-to-qubit mapping with the ratio $r = 1.5$ [8].

In this work, we focus on lattices in two spatial dimensions. First, we construct a new super-compact fermion-to-qubit mapping with the qubit-fermion ratio $r = 1.25$ on the 2d square lattice. Moreover, we provide a systematic approach to construct various 2d bosonizations by utilizing the ideas of Clifford circuit [22, 23] and finite-depth generalized local unitary (gLU) transformations [24, 25]. Such an approach provides a new perspective to study the relationship between different fermion-to-qubit mappings. We find that all the local fermion-to-qubit mappings can be generated from the exact bosonization by finite-depth gLU transformations. In particular, we explicitly show how to obtain the Bravyi-Kitaev superfast encoding (BKSF), the Verstraete-Cirac mapping, Kitaev’s honeycomb model, the Majorana loop stabilizer codes (MLSC), and the compact fermion-to-qubit mapping.

Summary of results

We first demonstrate a super-compact fermion-to-qubit mapping on the 2d square lattice with qubit-fermion ratio $r = 1.25$ in Sec. II and compare its data with other fermion-to-qubit mappings in Table I. In Sec. III, we define the crucial theoretical technique in our construction: the generalized local unitary (gLU) transformation [24, 25]. Then, in Sec. IIIB, we derive the $r = 1.5$ fermion-to-qubit mapping, which is equivalent to the compact encoding [8]. In Sec. IIIC, we further improve the ratio to derive the $r = 1.25$ construction shown in the previous section. In Sec. IIID, we prove that a general construction with ratio $r = 1 + \frac{1}{2k}$ exists for any positive integer k . The proof utilizes the trivialness of 2d quantum cellular automata (QCA) [26, 27]. In Sec. IV, we define the equivalence relation between different 2d bosonizations based on finite-depth gLU trans-

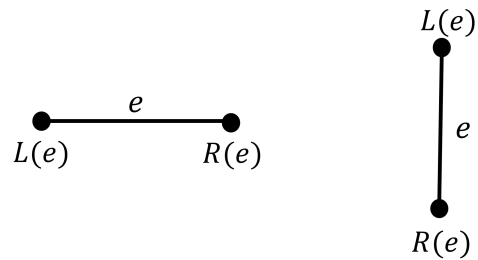


FIG. 1. Definition of left and right along horizontal and vertical edges

formations and discuss the equivalence between the exact bosonization and many well-known fermion-to-qubit mappings. We construct explicit Clifford circuits that convert the exact bosonization to the Bravyi-Kitaev superfast encoding (Sec. IV A), the Verstraete-Cirac mapping (Sec. IV B), Kitaev’s honeycomb model (Sec. IV C), the Majorana loop stabilizer codes (Sec. IV D), and the Jordan-Wigner transformation (Sec. IV E).

II. SUPER-COMPACT FERMION-TO-QUBIT MAPPING

In this section, we introduce a super-compact encoding of fermions by qubits with the qubit-fermion ratio $r = 1.25$. We first introduce the Hilbert spaces for fermions and qubits and then describe the mapping between them.

On the 2d square lattice in Fig. 2, each vertex v contains a fermionic mode with creation/annihilation operator c_v^\dagger, c_v with the standard commutation relation $\{c_v, c_{v'}^\dagger\} = \delta_{vv'}$. It is easier to use the Majorana basis

$$\gamma_v = c_v + c_v^\dagger, \quad \gamma'_v = \frac{c_v - c_v^\dagger}{i}. \quad (1)$$

The local fermion parity operator at a vertex v is

$$B_v \equiv (-1)^{c_v^\dagger c_v} = -i\gamma_v \gamma'_v, \quad (2)$$

and the hopping operator on an edge e is

$$A_e = i\gamma_{L(e)}\gamma_{R(e)}, \quad (3)$$

where $L(e)$ and $R(e)$ are the left and right vertices of the edge e defined in Fig. 1. The even algebra of fermions consists of local observables with a trivial fermion parity, i.e., local observables which commute with the total fermion parity $(-1)^F \equiv \prod_f (-1)^{c_f^\dagger c_f}$.² The generators for the even algebra of fermions are A_e and B_v on all edges and vertices [1].

² The even fermionic algebra can also be considered as the algebra of local observables containing an even number of Majorana operators.

	qubit-fermion-ratio r	fermion parity weight	hopping weight	stabilizer weight
Verstraete-Cirac [2] ^a	2	1	3-4	6
BKSF [10] ^b	2	4	2-6	6
Kitaev's honeycomb model [3]	2	2	2-5	6
Exact bosonization [1]	2	4	2-6	6
MLSC [5]	2	3	3-4	4-10
Compact fermion-to-qubit mapping [8]	1.5	1	3	8
Super-compact fermion-to-qubit mapping	1.25	1-2	2-6	12

^a The graph structure of the auxiliary Hamiltonian is Fig. 15.

^b The ordering of edges is shown in Fig. 14.

TABLE I. Comparison between fermion-to-qubit mappings on the 2d square lattice.

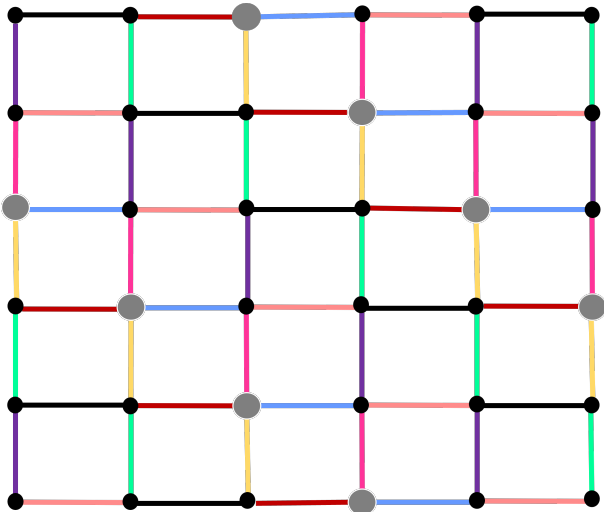


FIG. 2. The Hilbert space for the super-compact encoding. Each vertex encodes a fermionic mode, while each black vertex has 1 qubit and each grey vertex has 2 qubits. The qubit-fermion ratio r is 1.25 in this setting.

On the other hand, the qubits are put at vertices in Fig. 2. We label vertices by black and grey colors. For each black vertex, there is 1 qubit, and for each grey vertex, there are 2 qubits. As shown in Fig. 3 and 4, each grey vertex has two Pauli matrices on the top-right and bottom-left corners respectively.

The fermion-to-qubit mappings are mappings from A_e, B_v to Pauli strings (products of Pauli matrices) on qubits with the same algebra. In addition, such mapping satisfies a condition that the product of A_e along an arbitrary closed path should be the identity operator (up to a phase) since all Majorana operators cancel out. Such constraint requires the qubit system to be stabilized by a stabilizer group which is a set of hopping operators along with all closed loops. Now, we explicitly construct the mapping on the lattice in Fig. 2:

$$\begin{aligned} A_e &= i\gamma_{L(e)}\gamma_{R(e)} \longleftrightarrow \tilde{A}_e, \\ B_v &= -i\gamma_v\gamma'_v \longleftrightarrow \tilde{B}_v, \end{aligned} \quad (4)$$

where \tilde{A}_e and \tilde{B}_v are defined in Fig. 3. It can be checked that two operators \tilde{A}_e and $\tilde{A}_{e'}$ anti-commute if and only

if e and e' are two distinct edges sharing one common vertex, and \tilde{A}_e and \tilde{B}_v anti-commute if and only if the edge e contains the vertex v . Therefore, $\{A_e, B_v\}$ and $\{\tilde{A}_e, \tilde{B}_v\}$ satisfy the same commutation relations. The last step is to impose the stabilizer conditions (gauge constraints) that product of \tilde{A}_e on a loop l is proportional to the identity operator:

$$\prod_{e \in l} \tilde{A}_e = i^{|l|}, \quad (5)$$

where $|l|$ is the length of the loop l .

The generators of this stabilizer condition are expressed in Fig. 4. The stabilizers for the vertices that connect pink, black, green, purple edges generate the whole stabilizer group. The weight of such a stabilizer is 12.

III. GENERALIZED LOCAL UNITARY CIRCUITS ON THE EXACT BOSONIZATION

We describe a systematical way to derive fermion-to-qubit mappings from the exact bosonization in two spatial dimensions in the section. In Ref. [1], the exact bosonization is proposed using the subspace of the toric code with fermionic excitations, which will be reviewed in Sec. III A. By applying local unitary operators on the exact bosonization, we can generate a new fermion-to-qubit mapping. However, to include the lattice deformation or changing of the Hilbert spaces, local unitary operators are not sufficient, and the idea of generalized local unitary (gLU) operators is introduced.

The generalized local unitary (gLU) [24, 25] arises from the idea of wave function renormalization where local unitary operators are used to add or remove degrees of freedom at different length scales. For a wave function, we can use an operation to add or remove ancilla qubits in the product state.³ We call the transformation that changes the degrees of freedom a generalized

³ Since the ancilla qubits are in the products, adding or removing them do not change the information contained in the state.

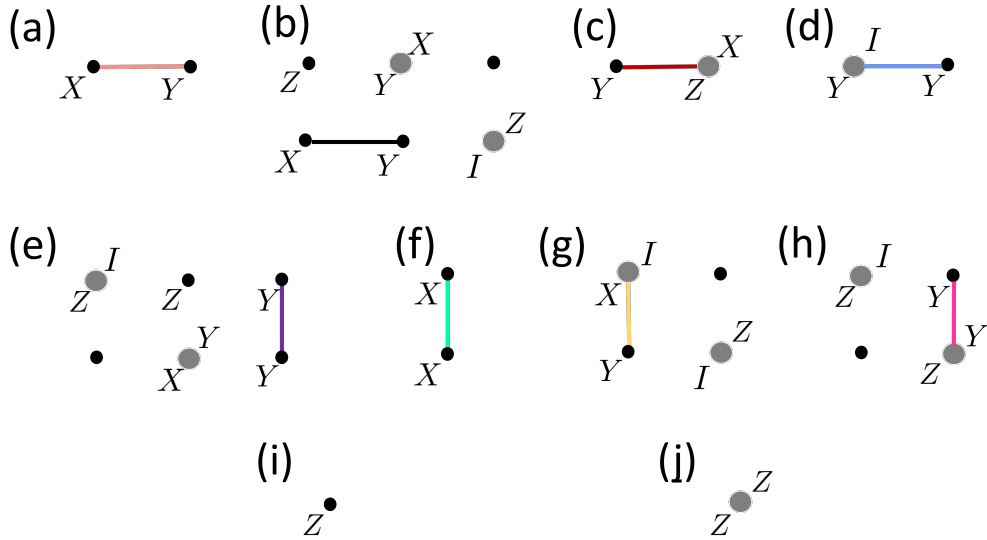


FIG. 3. The hopping term \tilde{A}_e and the parity term \tilde{B}_v in the bosonic Hilbert space. The definition of \tilde{A}_e and \tilde{B}_v depend on the colors of edges and vertices. (a),(b),(c),(d) are four kinds of horizontal hopping terms; (e),(f),(g),(h) are four kinds of vertical hopping terms; (i), (j) are parity terms on black and grey vertices.

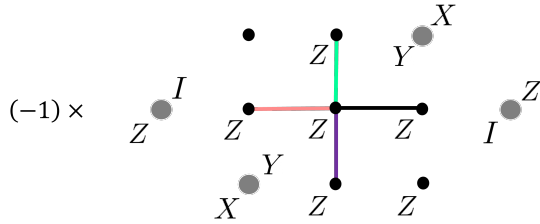


FIG. 4. The stabilizer acts on the vertex that connects to pink, black, purple, and green edges. The product of \tilde{A}_e on any closed loop is generated by this stabilizer.

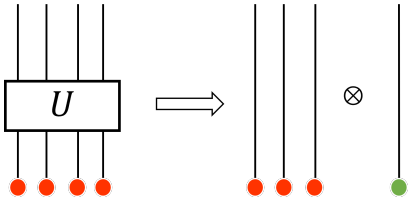


FIG. 5. We disentangle the green qubit from others by a local unitary transformation U and then discard this part. This is called a generalized local unitary circuit.

local unitary (gLU) operator. The formal definition of gLU in Ref. [24] is as follows. For a quantum state $|\Phi\rangle$ with the reduced density matrix ρ_A in region A , ρ_A only acts in a support subspace V_A^{sp} of the total Hilbert space \mathcal{H}_A . The dimension of V_A^{sp} is D_A^{sp} , which is called support dimension. Hence, the total Hilbert space on region A can be written as a direct sum $\mathcal{H}_A = V_A^{sp} \oplus \bar{V}_A^{sp}$. Let $|\tilde{\psi}_i\rangle$, $i = 1, \dots, D_A^{sp}$ to be the basis of V_A^{sp} , $|\tilde{\psi}_i\rangle$, $i = D_A^{sp} + 1, \dots, D_A$ to be the basis of \bar{V}_A^{sp} , and $|\psi_i\rangle$, $i = 1, \dots, D_A$ to be the basis of \mathcal{H}_A ($D_A = \dim(\mathcal{H}_A)$).

We introduce the local unitary transformation U^{full} to rotate $|\psi_i\rangle$ to $|\tilde{\psi}_i\rangle$. In the new basis, wave function $|\Phi\rangle$ only has non-zero amplitudes on the first D_A^{sp} basis vectors, and therefore we can truncate out the remaining columns of U^{full} to get the gLU operator U without losing any information.

With gLU transformation, we can remove the degrees of freedom in the system if they are in the product states. This operation is equivalent to disentangling parts of qubits from others. Hence, the qubit-fermion ratio r can be improved by wisely applying finite-depth gLU to the exact bosonization. In this paper, we will use finite-depth gLU Clifford circuits since we focus on Pauli stabilizer models. We demonstrate the construction of fermion-to-qubit mappings with ratio $r = 1.5$ in Sec. III B and $r = 1.25$ in Sec. III C by conjugating the 2d exact bosonization by certain finite-depth gLU Clifford circuits.

A. Review of the exact bosonization

We review the exact bosonization on the Hilbert space defined in Fig. 6. The elements of vertices, edges, and faces are denoted v, e, f . On each face f of the lattice we place a single pair of fermionic creation-annihilation operators c_f, c_f^\dagger , or equivalently a pair of Majorana fermions γ_f, γ_f' . The even fermionic algebra consists of local observables with a trivial fermion parity, i.e., local observables which commute with the total fermion parity $(-1)^F \equiv \prod_f (-1)^{c_f^\dagger c_f}$. The even algebra is generated by [1]:

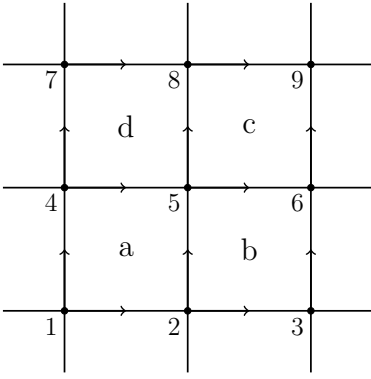


FIG. 6. Bosonization on a square lattice [1]. We put Pauli matrices X_e, Y_e, Z_e on each edge and one complex fermion c_f, c_f^\dagger at each face. We work on the Majorana basis $\gamma_f = c_f + c_f^\dagger$ and $\gamma'_f = -i(c_f - c_f^\dagger)$ for convenience.

1. On-site fermion parity:

$$P_f \equiv -i\gamma_f\gamma'_f. \quad (6)$$

2. Fermionic hopping term:

$$S_e \equiv i\gamma_{L(e)}\gamma'_{R(e)}, \quad (7)$$

where $L(e)$ and $R(e)$ are faces to the left and right of e , with respect to the orientation of e in Fig. 6.

The bosonic dual of this system involves \mathbb{Z}_2 -valued spins on the edges of the square lattice. For every edge e , we define a unitary operator U_e that squares to 1. Labeling the faces and vertices as in Fig. 6, we define:

$$\begin{aligned} U_{56} &= X_{56}Z_{25}, \\ U_{58} &= X_{58}Z_{45}, \end{aligned} \quad (8)$$

where X_e, Z_e are Pauli matrices acting on a spin at each edge e . Operators U_e for other edges are defined by using translation symmetry. Pictorially, the operator U_e is drawn as

$$U_e = \begin{array}{c} | \\ X_e \\ -Z- \end{array} \quad \text{or} \quad \begin{array}{c} -X_e- \\ | \\ Z \end{array}, \quad (9)$$

corresponding to the vertical or horizontal edge e .

It has been shown in Ref. [1] that U_e and S_e satisfy the same commutation relations. We also map the fermion parity P_f at each face f to the “flux operator” $W_f \equiv \prod_{e \subset f} Z_e$, the product of Z_e around a face f :

$$W_f = \begin{array}{c} -Z- \\ | \\ Z \quad f \quad Z \\ | \\ -Z- \end{array}. \quad (10)$$

The bosonization map is

$$\begin{aligned} S_e &\longleftrightarrow U_e, \\ P_f &\longleftrightarrow W_f, \end{aligned} \quad (11)$$

or pictorially

$$i \times \frac{\gamma_{L(e)}}{\gamma'_{R(e)}} e \longleftrightarrow \begin{array}{c} -X_e- \\ | \\ Z \end{array}, \quad (12)$$

$$i \times \gamma_{L(e)} \left| \begin{array}{c} e \\ \gamma'_{R(e)} \end{array} \right. \longleftrightarrow \begin{array}{c} X_e \\ -Z- \end{array}, \quad (13)$$

$$-i\gamma_f\gamma'_f \longleftrightarrow \begin{array}{c} -Z- \\ | \\ Z \quad f \quad Z \\ | \\ -Z- \end{array}. \quad (14)$$

The condition $P_a P_c S_{58} S_{56} S_{25} S_{45} = 1$ on fermionic operators gives gauge constraints (stabilizer) $G_v = W_{f_c} \prod_{e \supset v} X_e = 1$ for bosonic operators, or generally

$$G_v = \begin{array}{c} -Z- \\ | \\ XZ \quad f \quad Z \\ | \\ -X- v -XZ- \\ | \\ X \end{array} = 1. \quad (15)$$

The gauge constraint Eq. (15) can be considered as the stabilizer ($G_v |\Psi\rangle = |\Psi\rangle$ for $|\Psi\rangle$ in the code space), which forms the stabilizer group \mathcal{G} . The operators U_e and W_f generate all logical operators.⁴ In the setting above, qubits live on edges and fermions live on faces, so the ratio between the number of qubits and the number of fermions is $r = 2$. We are going to apply finite-depth gLU transformations to lower this ratio.

B. Compact fermion-to-qubit mapping with ratio $r = 1.5$

In the exact bosonization on the square lattice, the bosonic subspace is constrained by the stabilizer Eq. (15) at each vertex. First, we enlarge the unit cell to be a 2×2 square

$$\begin{array}{|c|c|} \hline \text{even} & \text{odd} \\ \hline \text{odd} & \text{even} \\ \hline \end{array}. \quad (16)$$

⁴ The logical operators consist of all operators that commute with \mathcal{G} . \mathcal{G} are trivial logical operators since stabilizers have no effect on the code space. U_e and W_f generate all logical operators.

Note that we have colored the faces to be even or odd as the checkerboard. In each 2×2 square, there are totally 4 fermions, 8 qubits and 4 stabilizers, whose qubit-fermion ratio is $r = \frac{8}{4} = 2$. We are going to apply a finite-depth gLU circuit to disentangle some qubits and reduce the ratio.

In Fig. 7, the translational invariant Clifford circuit is defined.⁵ We divide the stabilizers into two cases, living on an odd face or an even face, as shown below

$$G_{\text{odd}} = \begin{array}{c} \text{---Z---} \\ | \\ XZ \text{ odd } Z \\ | \\ -X- -XZ- \\ | \\ X \end{array}, \quad G_{\text{even}} = \begin{array}{c} \text{---Z---} \\ | \\ XZ \text{ even } Z \\ | \\ -X- -XZ- \\ | \\ X \end{array}.$$

After the conjugation of the Clifford circuit in Fig. 7, these stabilizers become

$$\begin{array}{c} \text{---Z---} \\ | \\ XZ \text{ odd } Z \\ | \\ -X- -XZ- \\ | \\ X \end{array} \longrightarrow (-1) \times \begin{array}{c} \text{---} \\ | \\ Y \text{ odd} \\ | \\ \text{---} \\ | \\ \text{---} \end{array}, \quad (17)$$

$$\begin{array}{c} \text{---Z---} \\ | \\ XZ \text{ even } Z \\ | \\ -X- -XZ- \\ | \\ X \end{array} \longrightarrow (-1) \times \begin{array}{c} \text{---} \\ | \\ Y \text{ even} \\ | \\ -X- -X- \\ | \\ Z \\ | \\ -X- -X- \\ | \\ Y \end{array}. \quad (18)$$

We have converted the stabilizer G_{odd} into a single-qubit stabilizer Y . This qubit will be in the eigenstate of Y and can be discarded. Hence, we successfully eliminate the qubits on the left edges of all odd faces. In the 2×2 unit square Eq. (16), there are only 6 qubits remaining, and the ratio between qubits and fermions is $\frac{6}{4} = 1.5$.

By the Clifford circuits in Fig. 7, we eliminate stabilizers on odd faces and convert the stabilizers on even faces to toric-code-like stabilizers. Next, we analyze the logical operators which represent the hopping of fermion after the conjugation. Here the convention of the fermionic hopping is $S_e \equiv i\gamma_{L(e)}\gamma'_{R(e)}$. There are four types of

fermionic hopping operator (after removing the degrees of freedom in Eq. (17))

$$\begin{array}{c} \text{---} \\ | \\ \text{odd } X_e \\ | \\ \text{---Z---} \end{array} \longrightarrow \begin{array}{c} \text{---Z---} \\ | \\ \text{odd } X_e \\ | \\ \text{---Z---} \end{array},$$

$$\begin{array}{c} \text{---} \\ | \\ \text{even } X_e \\ | \\ \text{---Z---} \end{array} \longrightarrow \begin{array}{c} \text{---Z---} \\ | \\ \text{even } e \\ | \\ -Y- -X- \\ | \\ Y \end{array}, \quad (19)$$

$$\begin{array}{c} \text{---} \\ | \\ Z \text{ odd} \\ | \\ \text{---} \end{array} \longrightarrow \begin{array}{c} \text{---} \\ | \\ \text{odd} \\ | \\ \text{---} \end{array},$$

$$\begin{array}{c} \text{---} \\ | \\ Z \text{ even} \\ | \\ \text{---} \end{array} \longrightarrow \begin{array}{c} \text{---} \\ | \\ \text{even} \\ | \\ \text{---} \end{array},$$

and two types of flux operators

$$\begin{array}{c} \text{---Z---} \\ | \\ Z \text{ odd } Z \\ | \\ \text{---Z---} \end{array} \longrightarrow \begin{array}{c} \text{---Z---} \\ | \\ \text{odd } Z \\ | \\ \text{---Z---} \end{array}, \quad (20)$$

$$\begin{array}{c} \text{---Z---} \\ | \\ Z \text{ even } Z \\ | \\ \text{---Z---} \end{array} \longrightarrow \begin{array}{c} \text{---Z---} \\ | \\ Z \text{ even} \\ | \\ \text{---Z---} \end{array}.$$

We note that the stabilizer in Eq. (18) is the same as the stabilizer of the compact encoding in Ref. [8] (up to the relabeling of Pauli matrices X, Y, Z). Since the stabilizers are the same, the space of logical operators must be equivalent. We can redefine the bottom two lines of Eq. 19 as “fermion parity” by re-pairing of Majorana fermions as Fig. 8, and reproduce the compact encoding in Ref. [8].

C. Super-compact fermion-to-qubit mapping with ratio $r = 1.25$

Based on the $r = 1.5$ construction in the previous section, which is obtained from conjugating the original 2d bosonization by the Clifford circuit shown in Fig. 7, we further conjugate it by the Clifford circuit in Fig. 10. In the $r = 1.5$ construction, we label squares by “even” and “odd”. Since the translational invariant Clifford circuit in Fig. 10 acts on a 2×2 cell, we color squares by 4 different colors: yellow, blue, red, and green and call them class 1, 2, 3, and 4 squares. Classes 1 and 3 belong to

⁵ We have enlarged the unit cell and therefore the distances for the translational generators are doubled.

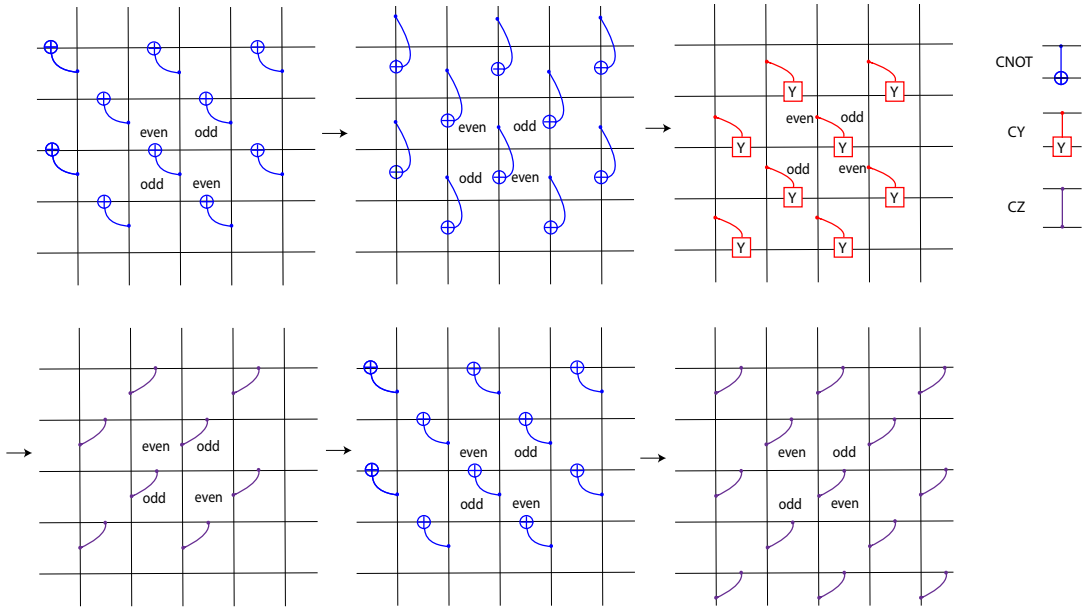


FIG. 7. The finite-depth Clifford circuit for the $r = 1.5$ construction

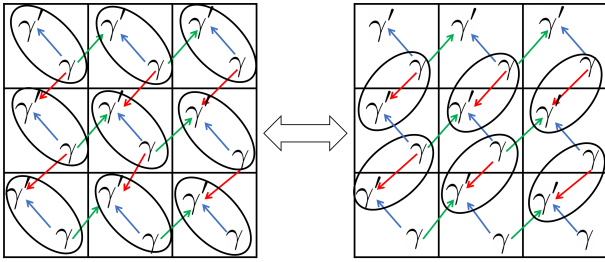


FIG. 8. The $r = 1.5$ construction is the same as the compact fermion-to-qubit mapping [8] after the re-pairing of Majorana fermions above. Each circle represents a complex fermion generated by the two Majorana fermions. The underlying arrows specify the order to form a fermion. This is a Kasteleyn orientation ensuring the re-pairing is well-defined [28].

“odd” faces, while classes 2 and 4 belong to the “even” faces.

Conjugated by the circuits in Fig. 10, the stabilizers enveloping blue and yellow squares become

$$(-1) \times \begin{array}{cccc} \circ & \circ & \circ & \circ \\ \circ & \circ & \circ & \circ \\ \circ & \circ & \circ & \circ \\ \circ & \circ & \circ & \circ \end{array} \longrightarrow (-1) \times \begin{array}{cccc} X & & & \\ \circ & Y & Y & \circ \\ \circ & \circ & Y & \circ \\ Z & Y & Y & X \\ \circ & Y & Y & \circ \\ \circ & \circ & Y & \circ \\ & & & Z \end{array}$$

However, the stabilizers enveloping green and red

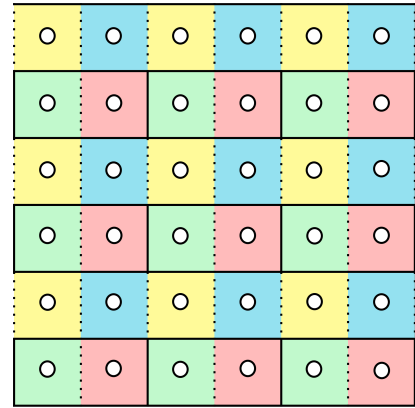


FIG. 9. Square lattice, yellow squares are in class 1; blue squares are in class 2; red squares are in class 3; green squares are in class 4. Dots are fermionic modes encoded inside squares. Each solid line has one qubit. There are no qubits on dashed lines.

squares become

$$(-1) \times \begin{array}{cccc} \circ & Y & \circ & \circ \\ X & X & \circ & \circ \\ Z & \circ & Z & \circ \\ X & X & \circ & \circ \\ \circ & Y & \circ & \circ \\ \circ & \circ & \circ & \circ \end{array} \longrightarrow (-1) \times \begin{array}{cccc} \circ & \circ & \circ & \circ \\ \circ & \circ & \circ & \circ \\ \circ & Y & \circ & \circ \\ \circ & \circ & \circ & \circ \\ \circ & \circ & \circ & \circ \end{array}$$

which is trivial. Then, we can simply remove the qubits on the boundaries between yellow and blue squares, which reduces the qubit-fermion ratio to $r = 1.25$.

Similarly, we conjugate Eq. (19) and (20) by the Clifford circuit in Fig. 10, and the result of these logical operators are listed in Fig. 11. This gives the super-compact fermion-to-qubit mapping demonstrated in Sec. II by a

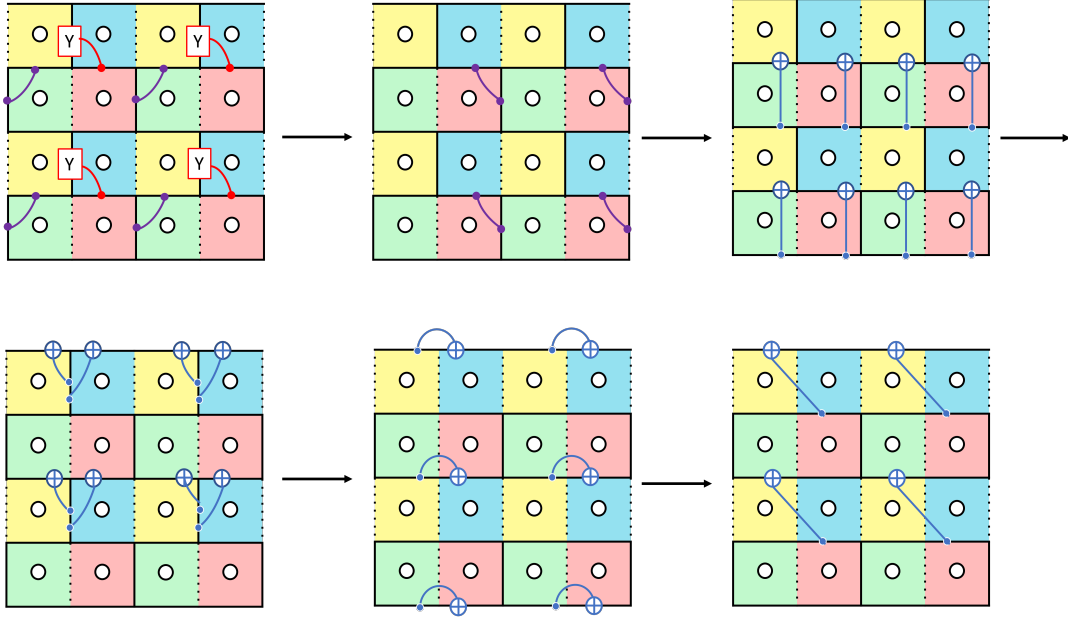


FIG. 10. The finite-depth Clifford circuit to construct bosonization with $r = 1.25$.

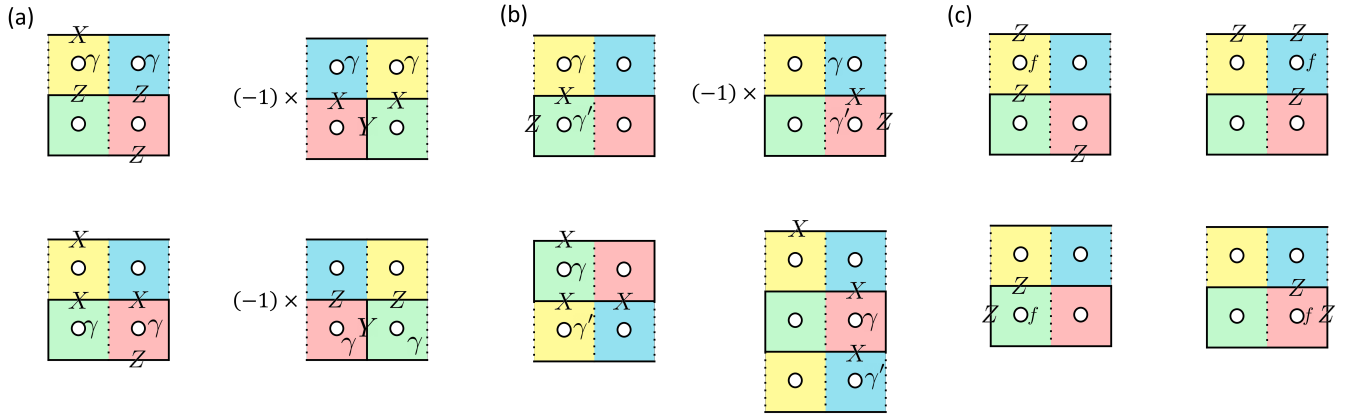


FIG. 11. (a) represents the nearest-neighbor horizontal hopping terms; (b) represents the near-neighbor vertical hopping terms; (c) represents the fermion parity operators

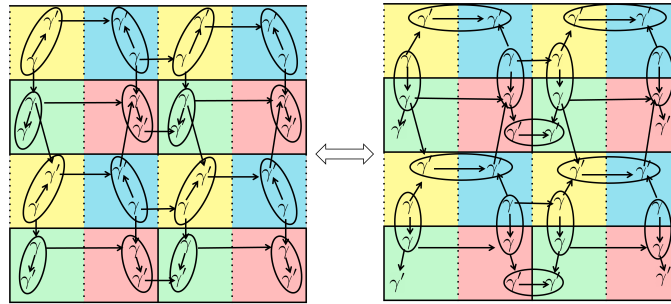


FIG. 12. The super-compact fermion-to-qubit mapping is the $r = 1.25$ construction after the fermion re-pairing. The arrows specify the order to form a complex fermion by two Majorana fermions in a circle. The arrows form a Kasteleyn orientation [29].

re-pairing of Majorana fermions (Fig. 12) and a slight lattice deformation.

D. General Construction for compact fermion-to-qubit mappings

In this section, we describe a general method to construct fermion-to-qubit mappings with a reduced qubit-fermion ratio from the exact bosonization. The exact bosonization contains gauge constraints (stabilizers) Eq. (15) supported on faces f (northeast to vertices v), and we rename G_v as G_f for convenience. We enlarge the unit cell and will show that it is always possible to apply finite-depth gLU operators such that a portion of stabilizers can be mapped to a single Pauli matrix. More precisely, we are going to prove that the stabilizer on each white face below can be mapped to a single Pauli matrix:

$$(21)$$

where k can be any positive integer.⁶

Instead of transforming G_f on white faces directly, we are going to prove a stronger statement: the gauge constraints G_f (Eq. (15)) on white faces, the hopping operators U_e (Eq. (42)) across horizontal edges, and the operators

$$G'_f \equiv \left[\begin{array}{c|c|c} \hline & \text{---}Y\text{---} & \\ \hline f & X & Z \\ \hline \end{array} \right], \quad (22)$$

on grey faces, can all be mapped to a single Pauli matrix simultaneously under a finite-depth gLU circuit. These

operators on the square lattice are shown as

$$(23)$$

To prove the above statement, we need to introduce a lemma:

Lemma 1. *Given \tilde{Z}_e and \tilde{X}_e for all edges that are products of Pauli matrices on a neighborhood of the edge e satisfying the Pauli algebra,*

$$[\tilde{X}_e, \tilde{X}_{e'}] = [\tilde{Z}_e, \tilde{Z}_{e'}] = 0, \quad \tilde{X}_e \tilde{Z}_{e'} = (-1)^{\delta_{e,e'}} \tilde{Z}_{e'} \tilde{X}_e,$$

there exists a finite-depth gLU transformation mapping \tilde{X}_e, \tilde{Z}_e to X_e, Z_e (a single Pauli on edge e).

Proof. The (Clifford) quantum cellular automata (QCA) in two spatial dimensions are simply (Clifford) local unitary circuits and shifts [26, 27]. The map α

$$\alpha(X_e) = \tilde{X}_e, \quad \alpha(Z_e) = \tilde{Z}_e, \quad (24)$$

defines a QCA and therefore can be decomposed to a Clifford circuit and shifts. For the shift operator, we can introduce ancilla in the $|0\rangle$ states and define the shift operator moving the ancilla in the opposite direction, such that the net flow of qubits is zero. Then, this shift operator can be expressed by a local unitary circuit (involving the ancilla degrees of freedom). In the end, these ancilla are still in the $|0\rangle$ states and can be removed by a finite-depth gLU transformation. Therefore, there exists a finite-depth gLU transformation from X_e, Z_e to \tilde{X}_e, \tilde{Z}_e and vice versa. \square

Lemma 2. *Given operators \tilde{Z}_e (separators) and \tilde{X}_e (flippers) that are products of Pauli matrices on a neighborhood of the edge e satisfying*

$$[\tilde{Z}_e, \tilde{Z}_{e'}] = 0, \quad \tilde{X}_e \tilde{Z}_{e'} = (-1)^{\delta_{e,e'}} \tilde{Z}_{e'} \tilde{X}_e, \quad (25)$$

there exist operators \tilde{X}_e that are products of Pauli matrices on a neighborhood of edges e such that

$$[\tilde{X}_e, \tilde{X}_{e'}] = [\tilde{Z}_e, \tilde{Z}_{e'}] = 0, \quad \tilde{X}_e \tilde{Z}_{e'} = (-1)^{\delta_{e,e'}} \tilde{Z}_{e'} \tilde{X}_e.$$

In other words, if the flippers do not commute with themselves, they can be modified such that the Pauli algebra is satisfied.

⁶ The portion of grey faces over all faces is $\frac{1}{2k}$. After removing stabilizers on white faces, the qubit-fermion ratio becomes $r = 1 + \frac{1}{2k}$.

Proof. If \bar{X}_e and $\bar{X}_{e'}$ do not commute,

$$\bar{X}_e \bar{X}_{e'} = -\bar{X}_{e'} \bar{X}_e, \quad (26)$$

we define

$$\tilde{X}_e \equiv \bar{X}_e \tilde{Z}_{e'}, \quad \tilde{X}_{e'} \equiv \bar{X}_{e'}. \quad (27)$$

Notice that $\tilde{Z}_{e'}$ only affects the commutation relation between e and e' and this fixes the commutation for the X part and leaves Z part unchanged. Therefore, \tilde{X}_e and \tilde{Z}_e satisfy the Pauli algebra. \square

The operators \tilde{Z}_e and \tilde{X}_e are called separators and flippers [30]. Once the separators and flippers are given, a QCA is defined by Eq. (24) (after defining \tilde{X}_e by Eq. (27)). By lemma 1, the separator can be mapped to a single Pauli matrix by a finite-depth gLU transformation.

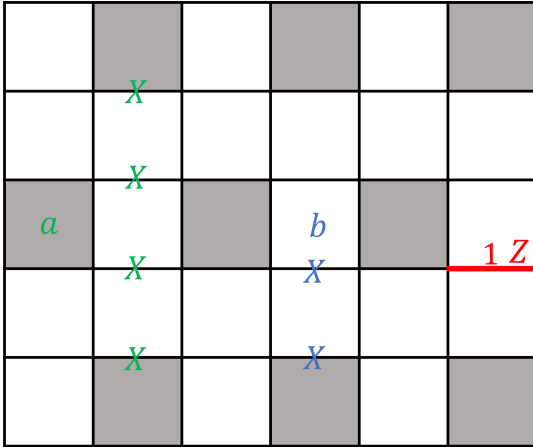


FIG. 13. The (potential) flippers. For G'_a on the grey face a , its flipper is the product of X connecting two grey faces on its right column, shown by the green operator. For G'_b on the white face, its potential flipper is the product of X connecting to a grey face below, shown by the blue operator. This potential flipper may anti-commute with G' on a grey face, which can be fixed by attaching the flipper for this G' . For U_{e_1} on a horizontal edge e_1 , the potential flipper is Z_{e_1} , which flips exactly one U_e and anti-commute with some G_f and G'_f on white and grey faces. This can be fixed by attaching the flippers for these G_f and G'_f to the potential flipper of U_{e_1} .

The operators G_f on white faces, U_e on horizontal edges, and G'_f in grey faces in (23) are the separators \tilde{Z}_e . Now, we are going to describe their flippers:

1. For G'_f on grey faces, we define its flippers by the product of X_e (m -strings of the toric code) connecting two grey faces on the column to the right, as shown in Fig. 13. It can be checked that this m -string only violates exactly one G'_f and commute with all other separators G_f and U_e .

2. A potential flipper⁷ for the separator G_f on a white face is the product of X connecting the white face to the grey face below (Fig. 13). This operator flips exactly one G_f on white faces and commutes with U_e , but it may anti-commute with a G'_f on a grey face. In this case, we can always attach the flipper for this G'_f (found in step 1) to the potential flipper. This operator becomes the true flipper for a single G_f .
3. For U_e on a horizontal edge, we start with a potential flipper Z on this edge e . It is obvious that it flips only one U_e and may anti-commute a finite number of G_f and G'_f on white and grey faces. Since we have already found the flippers for G_f and G'_f , we can attach these flippers to the potential flipper such that the combined operator commutes with all separators except one U_e .

We have found the complete set of separators and flippers on the square lattice. By Lemma 1, the G_f on each white face can be mapped to a single Pauli matrix.

IV. EQUIVALENCE BETWEEN FERMION-TO-QUBIT MAPPINGS AND THE EXACT BOSONIZATION

In this section, we argue that any locality preserving fermion-to-qubit mappings⁸ in two spatial dimensions can be connected to the exact bosonization by a finite-depth gLU transformation. First, given a fermion-to-qubit mapping, it must contain the flux operators \tilde{W} (images of the local fermion parity) and the gauge constraints \tilde{G} (images of the product of fermionic hopping terms in a small closed loop). On a torus, we can define a Pauli stabilizer code as

$$H = -\sum \tilde{G} - \sum \tilde{W}. \quad (28)$$

Over two large cycles of the torus, we have the 4-fold ground state degeneracy since we do not impose the fermionic constraints on the large cycles. The code distance is linear in the system size since the logical operator is the product of hopping along with the large cycles. It is proven in Ref. [31] that any translationally invariant Z_p Pauli stabilizer model with a linear code distance is decomposed by a local Clifford circuit of constant depth into a finite number of copies of the toric code for any prime p .⁹ Since the degeneracy is 4 on the

⁷ The potential flipper is an operator satisfying the algebra (25) partially. For example, it may anti-commute with extra separators $\tilde{Z}_{e'}$. This issue can be fixed by attaching other operators to this potential flipper.

⁸ To be precise, we consider the mapping between local fermionic observables and local products of Pauli matrices.

⁹ In this paper, we only work on qubits, which corresponds to $p = 2$. Therefore, the theorem in Ref. [31] is valid.

torus, the above stabilizer code Eq. (28) must be a single copy of toric code up to a Clifford circuit. Therefore, \tilde{G} and \tilde{W} are related to G_v and W_f in the exact bosonization in Sec. III A by a gLU transformation (since the toric code defined on different lattice should be related by gLU transformation to add or remove qubits).

In the following part of this section, we will explicitly demonstrate how to transform many well-known fermion-to-qubit mappings in literature to the exact bosonization.

A. Bravyi-Kitaev superfast simulation

The Bravyi-Kitaev superfast simulation (BKSF) in Ref. [10] is a method to encode fermionic operators into Pauli operators. BKSF encodes complex fermions at vertices v by qubits on edges e . The key idea of BKSF is to assign an arbitrary ordering of edges around each vertex and write down the logical operators according to the ordering. For vertex v , we label the edges connected to v by (v, i) , $i = 1, 2, 3, 4$ on 2d square lattice, shown in Fig. 14.

The logical operators \tilde{A}_e^{BK} and \tilde{B}_v^{BK} are defined as

$$\begin{aligned} \tilde{A}_e^{\text{BK}} &= X_e \prod_{(L(e), i) < (L(e), j)} Z_{L(e), i} \prod_{(R(e), k) < (R(e), l)} Z_{R(e), k}, \\ \tilde{B}_v^{\text{BK}} &= \prod_{e \supset v} Z_{(v, e)}, \end{aligned} \quad (29)$$

where $(L(e), j)$ is the label of edge e on the vertex $L(e)$, $(R(e), l)$ is the label of edge e on the vertex $R(e)$. The fermion-to-qubit mapping is

$$\begin{aligned} A_e &= i\gamma_{L(e)}\gamma_{R(e)} \longleftrightarrow \tilde{A}_e^{\text{BK}}, \\ B_v &= -i\gamma_v\gamma'_v \longleftrightarrow \tilde{B}_v^{\text{BK}}, \end{aligned} \quad (30)$$

where A_e and B_v are fermionic operators defined in Sec. II. The product of \tilde{A}_e^{BK} on any closed loop need to satisfy the condition Eq. (5) due to the identity for Majorana operators

By the convention in Fig. 14, we have:

$$i\gamma_{L(e)}\gamma'_{R(e)} \longleftrightarrow \tilde{A}_e^{\text{BK}}\tilde{B}_{R(e)}^{\text{BK}} = \begin{array}{c} \text{---}Y_e\text{---} \\ | \\ \text{---}Z\text{---} \end{array} \cdot \quad (31)$$

We notice that this is the same logical operator as the exact bosonization in the dual lattice after we relabel the Pauli matrices X and Y . The fermion parity terms in both cases are just a product of Z around a vertex (a face in the dual lattice), and therefore the BKSF approach with this ordering convention is the same as the exact bosonization.

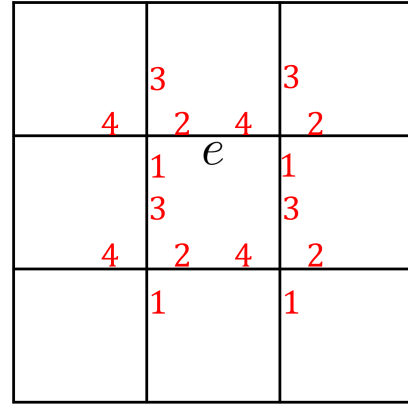


FIG. 14. The ordering of edges on each vertex. The red numbers are the labels.

B. Verstraete-Cirac auxiliary method

In this section, we demonstrate the equivalent relation between the Verstraete-Cirac mapping [2] and exact bosonization after regrouping Majorana fermions. The basic idea of the Verstraete-Cirac mapping is to eliminate the nonlocal Pauli Z -string from the 1d Jordan-Wigner transformation by introducing auxiliary qubits with gauge constraints. In this mapping, each site i uses four Majorana modes $\gamma_i, \gamma'_i, \tilde{\gamma}_i, \tilde{\gamma}'_i$ to encode a complex fermion and an auxiliary complex fermion. For implementation, we put two qubits on each vertex, one for the physical complex fermion, the other for the auxiliary complex fermion. The Majorana operators $\tilde{\gamma}_i, \tilde{\gamma}'_i$ belong to the auxiliary complex fermion. The auxiliary fermions stay in the ground state of following Hamiltonian

$$H_{aux} = \sum_{\{i, j\}} P_{ij} = i \sum_{\{i, j\}} \tilde{\gamma}_i \tilde{\gamma}'_j, \quad (32)$$

where the $\{i, j\}$ includes only pairs (i, j) that connected by the directed edges in Fig. 15. The hopping

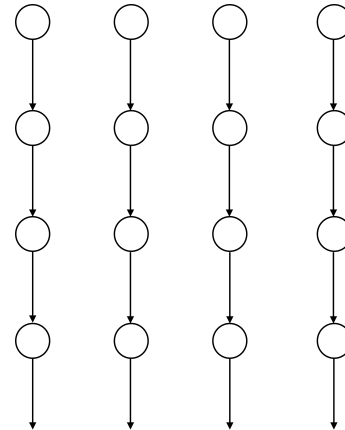


FIG. 15. Graph structure of the auxiliary Hamiltonian H_{aux} .

operator is modified as $c_i^\dagger c_j \rightarrow c_i^\dagger c_j (i\tilde{\gamma}_i \tilde{\gamma}'_j)$. We apply the 1d Jordan-Wigner transformation with ordering

$\{\gamma_{i_1}, \gamma'_{i_1}\} \rightarrow \{\tilde{\gamma}_{i_1}, \tilde{\gamma}'_{i_1}\} \rightarrow \{\gamma_{i_2}, \gamma'_{i_2}\} \rightarrow \{\tilde{\gamma}_{i_2}, \tilde{\gamma}'_{i_2}\} \rightarrow \dots$, where i_1, i_2, \dots in our convention start with the first row from left to right, and move to the second and so on. However, the auxiliary Hamiltonian is a non-local Hamiltonian. To resolve this problem, we perform following substitution $P_{\{N-1, N+2\}} \rightarrow P_{\{N-1, N+2\}} P_{\{N, N+1\}}$, $P_{\{N-2, N+3\}} \rightarrow P_{\{N-2, N+3\}} P_{\{N-1, N+2\}}$ for all rows. Since all P commute with each other, the auxiliary Hamiltonian H_{aux} becomes local without changes in the ground state. Then the local gauge constraint (stabilizer) is $P_{ij} = \tilde{\gamma}_i \tilde{\gamma}'_k \tilde{\gamma}_j \tilde{\gamma}'_l = 1$. The gauge constraint can be written as a Pauli stabilizer

$$P_{ik} = \begin{array}{c} | \\ I_i \\ | \\ -\tilde{X}_i- \\ | \\ I_k \\ | \\ -\tilde{Y}_k- \\ | \end{array} \begin{array}{c} | \\ Z_j \\ | \\ -\tilde{Y}_j- \\ | \\ Z_l \\ | \\ -\tilde{X}_l- \\ | \end{array} . \quad (33)$$

Pauli matrices $\{\tilde{X}_n, \tilde{Y}_n, \tilde{Z}_n\}$ act on the auxiliary qubit n . We put physical qubits on the vertical edges and auxiliary qubits on the horizontal edges. Since physical qubits and auxiliary qubits are in different edges, we will not show the tilde in following text for convenience.

Its hopping operators (S_e in Eq. (7)) and fermion parity operators (P_f in Eq. (6)) are

$$U_e = \begin{array}{c} | \\ X \\ | \\ -Y_e- \\ | \\ Y \\ | \\ -X- \\ | \end{array} , \quad \begin{array}{c} | \\ X \\ | \\ -Z- \\ | \\ X_e \\ | \end{array} \quad (34)$$

$$W_f = \begin{array}{c} | \\ \boxed{f} \\ | \\ Z \\ | \end{array} .$$

By conjugating the logical operators in Eq. (34) by the Clifford circuits shown in Fig. 16, the logical operators and stabilizer become

$$U_e = \begin{array}{c} | \\ e \\ | \\ -X- \\ | \\ Z \\ | \end{array} , \quad \begin{array}{c} | \\ -e- \\ | \\ X \\ | \\ -Z- \\ | \end{array}$$

$$W_f = \begin{array}{c} | \\ \boxed{f} \\ | \\ Y \\ | \end{array} \quad (35)$$

$$G_v = \begin{array}{c} | \\ -Z-v \\ | \\ XZ \\ | \\ -XZ- \\ | \\ X \\ | \end{array}$$

The logical operators and stabilizer in Eq. (35) is exactly the logical operators and stabilizers of exact bosonization after a shift of Majorana fermions. If we shift the Majorana fermions in the exact bosonization as Fig. 17 and re-pair them. Then we find the exact bosonization and the Verstraete-Cirac mapping are equivalent, as Fig. 18.

C. Kitaev's honeycomb model

The Hamiltonian of Kitaev's honeycomb model [3] can be written as

$$H = -J_x \sum_{x\text{-links}} X_j^A X_k^B - J_y \sum_{y\text{-links}} Y_j^A Y_j^B - J_z \sum_{z\text{-links}} Z_j^A Z_k^B, \quad (36)$$

where x, y, z links are shown in Fig. 19. The qubit at each site j can be represented by four Majorana operators b_j^x, b_j^y, b_j^z and γ_j with an additional constraint $b_j^x b_j^y b_j^z \gamma_j = 1$ to eliminate the redundancy at each site j . The Pauli matrices at each site j can be represented as follows:

$$X_j = ib_j^x \gamma_j, \quad Y_j = ib_j^y \gamma_j, \quad Z_j = ib_j^z \gamma_j, \quad (37)$$

or equivalently (after multiplying by D_j)

$$X_j = -ib_j^y b_j^z, \quad Y_j = -ib_j^z b_j^x, \quad Z_j = -ib_j^x b_j^y. \quad (38)$$

Then, a free-fermion Hamiltonian

$$H = \frac{i}{2} \sum_{e_{jk}} J_{\alpha_{jk}} \gamma_j^A \gamma_k^B \quad (39)$$

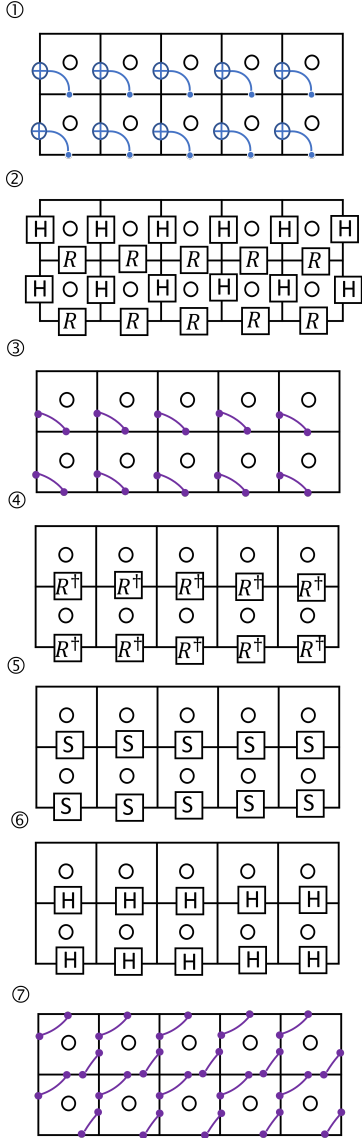


FIG. 16. The finite-depth Clifford circuit to convert the Verstraete-Cirac mapping to the exact bosonization. The details of H , R , S gates are discussed in Appendix A.

is equivalent to a sector of Eq. (36), where the index α takes values x , y or z depending on the direction of the link jk . Focusing on the algebra generated by γ_j , the mapping Eq. (37) can be written as [1]:

$$i\gamma_j^A \gamma_k^B \leftrightarrow \begin{cases} X_j^A X_k^B & \text{if } jk \in x\text{-link,} \\ Y_j^A Y_k^B & \text{if } jk \in y\text{-link,} \\ Z_j^A Z_k^B & \text{if } jk \in z\text{-link,} \end{cases} \quad (40)$$

and the product of Majorana hoppings along a hexagon is proportional to identity, which gives a gauge constraint on the qubit Hilbert space. It is shown [1] that by embedding the honeycomb lattice into the square lattice as Fig. 20, relabeling γ^A, γ^B by γ_f, γ'_f , and performing single-qubit rotations, the complete bosonization map

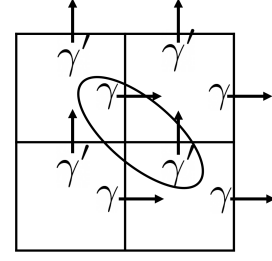


FIG. 17. To match our exact bosonization to Verstraete-Cirac mapping, we shift our Majorana modes on each face as following way: 1. shift γ'_f upward and let it be γ on the new face; 2. shift γ_f rightward and let it be γ' on the new face.

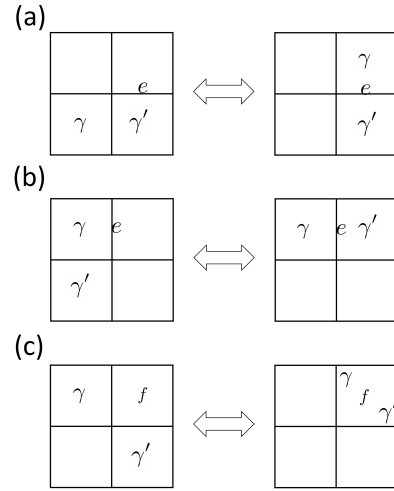


FIG. 18. Correspondence of logical operators between the exact bosonization and the Verstraete-Cirac mapping

can be expressed as

$$i \times \frac{\gamma_{L(e)}}{e} \leftrightarrow \begin{array}{c} \gamma_{R(e)} \\ -X_e \\ Z \end{array}, \quad (41)$$

$$i \times \gamma_{L(e)} \left| \begin{array}{c} e \\ \gamma'_{R(e)} \end{array} \right. \leftrightarrow \begin{array}{c} -Z \\ X_e \end{array}, \quad (42)$$

$$-i\gamma_f \gamma'_f \leftrightarrow \begin{array}{c} -Y \\ f \\ Y \end{array}, \quad (43)$$

with gauge constraints

$$G_v = \begin{array}{c} \text{---}Z\text{---} \\ | \\ XZ \quad f \quad Z \\ | \\ \text{---}X\text{---}v\text{---}XZ\text{---} \\ | \\ X \end{array} = 1. \quad (44)$$

This is equivalent to the logical operators and stabilizers in Eq. (35) up to a shift. Therefore, it is gLU equivalent to the exact bosonization.

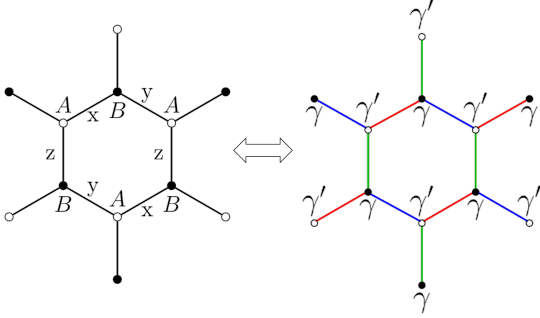


FIG. 19. Kitaev's honeycomb mapping between Pauli matrices and Majorana fermions. For each link, the product of two Pauli matrices on its vertices is mapped to the product of γ and γ' on its vertices by Eq. (40).

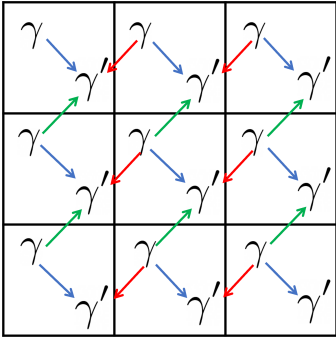


FIG. 20. The embedding of the honeycomb lattice in Fig. 19 to the square lattice.

D. Majorana loop stabilizer codes

In this section, we show that Majorana loop stabilizer code (MLSC) [5] is gLU equivalent to the 2d exact bosonization. Similar to BKSF, the Majorana loop stabilizer codes encode a complex fermion on vertex v by qubits on edge e connected to v . The Majorana loop stabilizer codes have fermionic hopping operation $A_e = i\gamma_{L(e)}\gamma_{R(e)}$ on each edge, fermion parity operator $P_f = -i\gamma_f\gamma'_f$ on each vertex and stabilizers G_v acting on

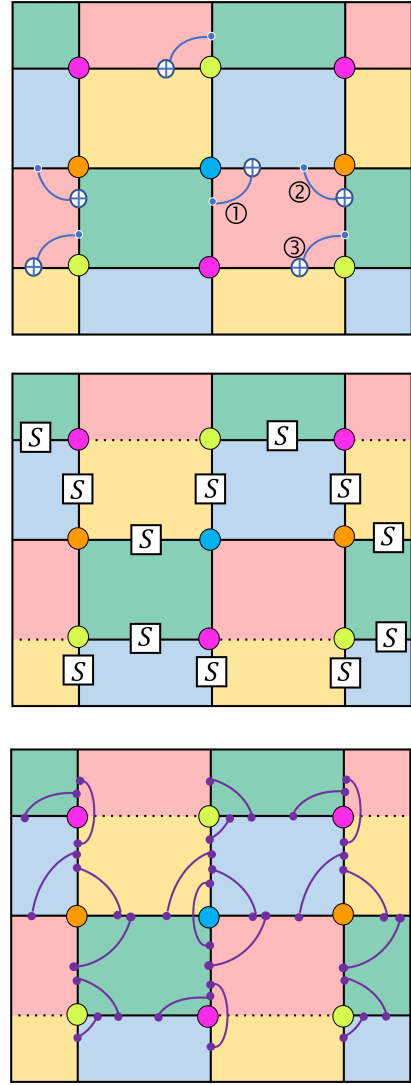


FIG. 21. The finite-depth Clifford circuit for the MLSC to the exact bosonization. The first Clifford circuit will disentangle the qubits on the edges between red and yellow squares, so the edges between red and yellow squares become dashed lines in the second and third steps.

faces with different colors. We follow the same procedure described in Sec. III, conjugating the logical operations and stabilizers of MLSC by finite-depth Clifford circuits in Fig. 21. Then the four kinds of horizontal hoppings in MLSC reduce to the horizontal hopping in the exact bosonization (up to a stabilizer), and the same thing happens to the vertical hoppings, parity operators, and stabilizers.

Starting from the MLSC, Fig. 22 and Fig. 23 shows that the horizontal and vertical hoppings $i\gamma_{L(e)}\gamma_{R(e)}$ after the transformation can match the horizontal and vertical hoppings in exact bosonization. An interesting fact is that the first Clifford circuit in Fig. 21 removes qubit on the edges between red and yellow squares and makes this correspondence possible.

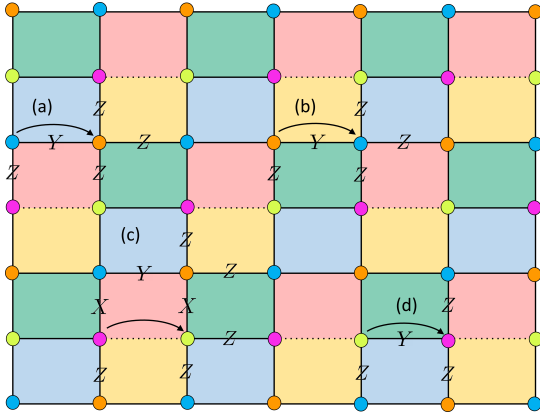


FIG. 22. Horizontal hopping $i\gamma_{L(e)}\gamma_{R(e)}$ after a finite-depth gLU transformation in Fig. 21. (a),(b) are hoppings between blue and orange dots; (c),(d) are hoppings between pink and yellow dots. (a),(b), (d) are exactly the horizontal hopping in the exact bosonization, and (c) is a product of the hopping operator and the stabilizer in the exact bosonization.

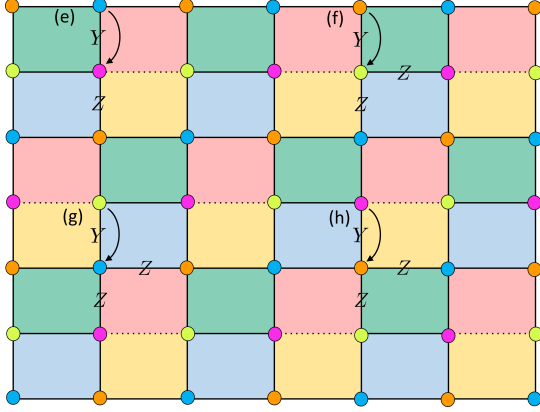


FIG. 23. (e),(f),(g) and (h) are the vertical hopping $i\gamma_{L(e)}\gamma_{R(e)}$ after a finite-depth gLU transformation in Fig. 21. They match the vertical hoppings in the exact bosonization.

E. Connection to Jordan-Wigner transformation

In this section, we will show that conjugating the exact bosonization by a linear-depth¹⁰ Clifford circuit in Fig. 24 will result in the 1d Jordan-Wigner transformation along the path in Fig. 25.

For the Jordan-Wigner transformation, the qubit-fermion ratio is 1, but it is a non-local fermion-to-qubit mapping since in 1d Jordan-Wigner transformation, the

vertical hopping terms are mediated by a Pauli Z -string between two sites. By directly applying the linear-depth gLU Clifford circuit in Fig. 24 to the logical operators of the exact bosonization, the qubits on the horizontal edges are disentangled and do not show up in the logical operators. All stabilizers become single-Pauli operators on horizontal edges and can be removed by gLU transformations. Explicitly, the logical operators after conjugation of the Clifford circuit are:

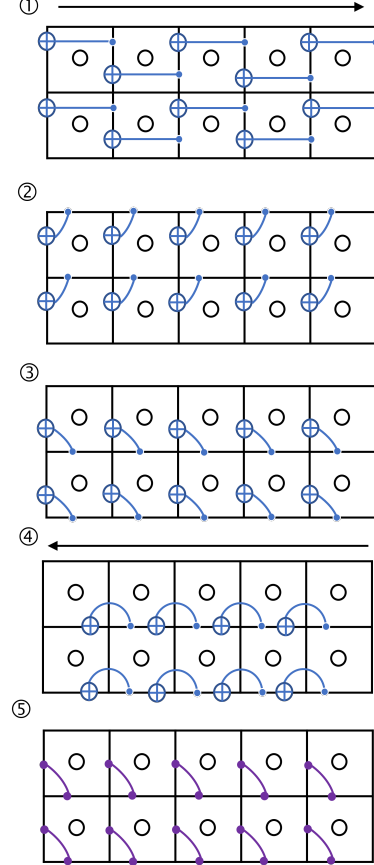


FIG. 24. The finite-depth Clifford circuit to convert the exact bosonization to 1d Jordan-Wigner transformation. In the first step, we ordered the system from the left to the right, then apply CNOT gate to each individual column following the above ordering. In the second step and third steps, the CNOT gates are applied simultaneously. In the fourth step, we order the system from the right to the left, then apply CNOT gate to each individual column following the right-to-left ordering. In the fifth step, CZ gates are simultaneously applied.

¹⁰ The depth of the circuit scales linearly with the system size.

$$\begin{array}{c} | \\ \hline X_e \\ \hline -Z- \\ | \end{array} \longrightarrow \begin{array}{c} | \\ \hline X \quad \gamma \quad X_e \quad \gamma' \\ \hline | \end{array}, \quad (45)$$

$$\begin{array}{c} | \\ \hline -X_e- \\ \hline Z \\ | \end{array} \longrightarrow \begin{array}{c} | \\ \hline Z \quad Z \quad \dots \quad Z \quad Y \quad \gamma \\ \hline | \end{array} \begin{array}{c} \longleftarrow \\ \hline -e- \\ \hline | \end{array} \begin{array}{c} | \\ \hline Y \quad \gamma' \quad Z \quad Z \quad \dots \quad Z \\ \hline | \end{array}, \quad (46)$$

$$\begin{array}{c} | \\ \hline -Z- \\ \hline Z \quad f \quad Z \\ \hline -Z- \\ | \end{array} \longrightarrow \begin{array}{c} | \\ \hline Z \quad f \\ \hline | \end{array}. \quad (47)$$

which is exactly the 1d Jordan-Wigner transformation with the ordering chosen in Fig. 25. Hence, we can regard 1d Jordan-Wigner transformation as a special case that we remove all the qubits on the horizontal edges where the vertical hoppings are no longer local.

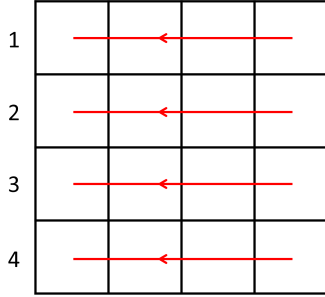


FIG. 25. Space ordering of 1d Jordan-Wigner transformation

ACKNOWLEDGEMENT

Y.-A.C thanks Mark Steudtner for pointing out the equivalence between the BKSF and the exact bosonization. Y.-A.C want to thank Anton Kapustin, Tyler Ellison and Nat Tantivasadakarn for useful discussions. Y.-A.C is also thankful to Bowen Yang for teaching the classification of Pauli stabilizer models in two dimensions. Y.-A.C is supported by the JQI fellowship at the University of Maryland. Y.X. is supported by ARO W911NF-15-1-0397 and advisor Mohammad Hafezi.

Appendix A: Clifford gates

The Clifford group is defined as the group of unitaries that normalize the Pauli group. The Clifford gates are defined as elements in the Clifford group [22, 23]. In

this paper, we use single-qubit Clifford gates: H -gate, S -gate, R -gate.

The H -gate is the Hadamard gate

$$H = \frac{1}{\sqrt{2}} \begin{bmatrix} 1 & 1 \\ 1 & -1 \end{bmatrix} \quad (A1)$$

that satisfies $HXH^\dagger = Z$, $HZH^\dagger = X$.

The S -gate is the phase gate

$$S = \begin{bmatrix} 1 & 0 \\ 0 & i \end{bmatrix} \quad (A2)$$

that satisfies $SXS^\dagger = Y$, $SY S^\dagger = -X$.

The R -gate is

$$R = \frac{1}{\sqrt{2}} \begin{bmatrix} 1 & i \\ i & 1 \end{bmatrix} \quad (A3)$$

where $RYR^\dagger = -Z$, $RZR^\dagger = Y$.

For 2-qubit Clifford gates, we choose $CNOT$, CY and CZ gate. The $CNOT$ gate is

$$CNOT = \begin{bmatrix} 1 & 0 & 0 & 0 \\ 0 & 1 & 0 & 0 \\ 0 & 0 & 0 & 1 \\ 0 & 0 & 1 & 0 \end{bmatrix}, \quad (A4)$$

where

$$\begin{aligned} CNOT(X \otimes I)CNOT^\dagger &= X \otimes X, \\ CNOT(Z \otimes I)CNOT^\dagger &= Z \otimes I, \\ CNOT(I \otimes X)CNOT^\dagger &= I \otimes X, \\ CNOT(I \otimes Z)CNOT^\dagger &= Z \otimes Z. \end{aligned} \quad (A5)$$

The CY (controlled- Y) gate is

$$CY = \begin{bmatrix} 1 & 0 & 0 & 0 \\ 0 & 1 & 0 & 0 \\ 0 & 0 & 0 & -i \\ 0 & 0 & i & 0 \end{bmatrix} \quad (\text{A6})$$

where

$$\begin{aligned} CY(X \otimes I)CY^\dagger &= X \otimes Y, \\ CY(Z \otimes I)CY^\dagger &= Z \otimes I, \\ CY(I \otimes X)CY^\dagger &= Z \otimes X, \\ CY(I \otimes Z)CY^\dagger &= Z \otimes Z. \end{aligned} \quad (\text{A7})$$

The CZ (controlled- Z) gate is

$$CZ = \begin{bmatrix} 1 & 0 & 0 & 0 \\ 0 & 1 & 0 & 0 \\ 0 & 0 & 1 & 0 \\ 0 & 0 & 0 & -1 \end{bmatrix} \quad (\text{A8})$$

where

$$\begin{aligned} CZ(X \otimes I)CZ^\dagger &= X \otimes Z, \\ CZ(Z \otimes I)CZ^\dagger &= Z \otimes I, \\ CZ(I \otimes X)CZ^\dagger &= Z \otimes X, \\ CZ(I \otimes Z)CZ^\dagger &= I \otimes Z. \end{aligned} \quad (\text{A9})$$

-
- [1] Yu-An Chen, Anton Kapustin, and Djordje Radicevic, “Exact bosonization in two spatial dimensions and a new class of lattice gauge theories,” *Annals of Physics* **393**, 234 – 253 (2018).
- [2] F Verstraete and J I Cirac, “Mapping local hamiltonians of fermions to local hamiltonians of spins,” *Journal of Statistical Mechanics: Theory and Experiment* **2005**, P09012–P09012 (2005).
- [3] Alexei Kitaev, “Anyons in an exactly solved model and beyond,” *Annals of Physics* **321**, 2–111 (2006).
- [4] James D. Whitfield, Vojt ěch Havlíček, and Matthias Troyer, “Local spin operators for fermion simulations,” *Phys. Rev. A* **94**, 030301 (2016).
- [5] Zhang Jiang, Jarrod McClean, Ryan Babbush, and Hartmut Neven, “Majorana loop stabilizer codes for error mitigation in fermionic quantum simulations,” *Physical Review Applied* **12** (2019), 10.1103/physrevapplied.12.064041.
- [6] Kanav Setia, Sergey Bravyi, Antonio Mezzacapo, and James D. Whitfield, “Superfast encodings for fermionic quantum simulation,” *Phys. Rev. Research* **1**, 033033 (2019).
- [7] A. Bochniak and B. Ruba, “Bosonization based on clifford algebras and its gauge theoretic interpretation,” *Journal of High Energy Physics* **2020**, 118 (2020).
- [8] Charles Derby, Joel Klassen, Johannes Bausch, and Toby Cubitt, “Compact fermion to qubit mappings,” *Phys. Rev. B* **104**, 035118 (2021).
- [9] Hoi Chun Po, “Symmetric jordan-wigner transformation in higher dimensions,” arXiv preprint arXiv:2107.10842 (2021).
- [10] Sergey B Bravyi and Alexei Yu Kitaev, “Fermionic quantum computation,” *Annals of Physics* **298**, 210–226 (2002).
- [11] Yu-An Chen and Anton Kapustin, “Bosonization in three spatial dimensions and a 2-form gauge theory,” *Phys. Rev. B* **100**, 245127 (2019).
- [12] Yu-An Chen, “Exact bosonization in arbitrary dimensions,” *Phys. Rev. Research* **2**, 033527 (2020).
- [13] Tyler D. Ellison and Lukasz Fidkowski, “Disentangling interacting symmetry-protected phases of fermions in two dimensions,” *Phys. Rev. X* **9**, 011016 (2019).
- [14] Yu-An Chen, Tyler D. Ellison, and Nathanan Tantivasadakarn, “Disentangling supercohomology symmetry-protected topological phases in three spatial dimensions,” *Phys. Rev. Research* **3**, 013056 (2021).
- [15] Yu-An Chen and Po-Shen Hsin, “Exactly solvable lattice hamiltonians and gravitational anomalies,” arXiv preprint arXiv:2110.14644 (2021).
- [16] Sergey Bravyi, Barbara M Terhal, and Bernhard Leemhuis, “Majorana fermion codes,” *New Journal of Physics* **12**, 083039 (2010).
- [17] Sagar Vijay and Liang Fu, “Physical implementation of a majorana fermion surface code for fault-tolerant quantum computation,” *Physica Scripta* **2016**, 014002 (2016).
- [18] Oscar Viyuela, Sagar Vijay, and Liang Fu, “Scalable fermionic error correction in majorana surface codes,” *Phys. Rev. B* **99**, 205114 (2019).
- [19] Sagar Vijay, Timothy H. Hsieh, and Liang Fu, “Majorana fermion surface code for universal quantum computation,” *Phys. Rev. X* **5**, 041038 (2015).
- [20] Daniel Litinski and Felix von Oppen, “Quantum computing with majorana fermion codes,” *Phys. Rev. B* **97**, 205404 (2018).
- [21] M. B. Hastings, “Small majorana fermion codes,” (2017), arXiv:1703.00612 [quant-ph].
- [22] Daniel Gottesman, “Theory of fault-tolerant quantum computation,” *Phys. Rev. A* **57**, 127–137 (1998).
- [23] Daniel Gottesman, “The heisenberg representation of quantum computers,” arXiv preprint quant-ph/9807006 (1998).
- [24] Xie Chen, Zheng-Cheng Gu, and Xiao-Gang Wen, “Local unitary transformation, long-range quantum entanglement, wave function renormalization, and topological order,” *Phys. Rev. B* **82**, 155138 (2010).
- [25] Bei Zeng, Xie Chen, Duan-Lu Zhou, and Xiao-Gang Wen, “Quantum information meets quantum matter – from quantum entanglement to topological phase in many-body systems,” (2018), arXiv:1508.02595 [cond-mat.str-el].
- [26] Michael Freedman and Matthew B. Hastings, “Classification of quantum cellular automata,” *Communications in Mathematical Physics* **376**, 1171–1222 (2020).
- [27] Jeongwan Haah, “Clifford quantum cellular automata: Trivial group in 2d and witt group in 3d,” *Journal of Mathematical Physics* **62**, 092202 (2021), <https://doi.org/10.1063/5.0022185>.
- [28] Nicolas Tarantino and Lukasz Fidkowski, “Discrete spin structures and commuting projector models for two-dimensional fermionic symmetry-protected topological phases,” *Phys. Rev. B* **94**, 115115 (2016).
- [29] Nicolas Tarantino and Lukasz Fidkowski, “Discrete spin structures and commuting projector models for two-dimensional fermionic symmetry-protected topological phases,” *Phys. Rev. B* **94**, 115115 (2016).
- [30] Jeongwan Haah, Lukasz Fidkowski, and Matthew B Hastings, “Nontrivial quantum cellular automata in higher dimensions,” arXiv preprint arXiv:1812.01625 (2018).
- [31] Jeongwan Haah, “Classification of translation invariant topological pauli stabilizer codes for prime dimensional qudits on two-dimensional lattices,” *Journal of Mathematical Physics* **62**, 012201 (2021), <https://doi.org/10.1063/5.0021068>.